

Suzaku Observation of Two Ultraluminous X-Ray Sources in NGC 1313

T. MIZUNO,¹ R. MIYAWAKI,² K. EBISAWA,³ A. KUBOTA,⁴ M. MIYAMOTO,⁵ L. WINTER,⁶
 Y. UEDA,⁷ N. ISOBE,⁴ G. DEWANGAN,⁸ C. DONE,⁹ R. E. GRIFFITHS,⁸ Y. HABA,¹⁰
 M. KOKUBUN,² J. KOTOKU,¹¹ K. MAKISHIMA,^{2,4} K. MATSUSHITA,⁵ R. F. MUSHOTZKY,⁶
 M. NAMIKI,¹² R. PETRE,⁶ H. TAKAHASHI,¹ T. TAMAGAWA,⁴ and Y. TERASHIMA^{*,3}

¹ *Department of Physics, Hiroshima University,*

1-3-1 Kagamiyama, Higashi-Hiroshima, Hiroshima 739-8526

mizuno@hepl.hiroshima-u.ac.jp

² *Department of Physics, University of Tokyo, 7-3-1 Hongo, Bunkyo-ku, Tokyo 113-0033*

³ *Institute of Space and Astronautical Science, Japan Aerospace Exploration Agency,*

3-1-1 Yoshinodai, Sagami-hara, Kanagawa 229-8510

⁴ *Institute of Physical and Chemical Research (RIKEN), 2-1 Hirosawa, Wako, Saitama 351-0198*

⁵ *Department of Physics, Tokyo University of Science, 1-3 Kagurazaka, Shinjuku-ku, Tokyo 162-8601*

⁶ *Exploration of the Universe Division, NASA Goddard Space Flight Center, Greenbelt, MD 20771, USA*

⁷ *Department of Physics, Kyoto University, Sakyo-ku, Kyoto 606-8502*

⁸ *Department of Physics, Carnegie Mellon University, 5000 Forbes Avenue, Pittsburgh, PA 15213, USA*

⁹ *Department of Physics, University of Durham, South Road, Durham, DH1 3LE, UK*

¹⁰ *Department of Physics, Nagoya University, Furo-cho, Chikusa, Nagoya 464-8602*

¹¹ *Department of Physics, Tokyo Institute of Technology, 2-12-1, Meguro-ku, Ohokayama, Tokyo 152-8551*

¹² *Department of Earth and Space Science, Osaka University,*

1-1 Machikaneyama-cho, Toyonaka, Osaka 560-0043

(Received 2006 August 4; accepted 2001 January 1)

Abstract

Two ultraluminous X-ray sources (ULXs) in the nearby Sb galaxy NGC 1313, named X-1 and X-2, were observed with Suzaku on 2005 September 15. During the observation for a net exposure of 28 ks (but over a gross time span of 90 ks), both objects varied in intensity by about 50 %. The 0.4–10 keV X-ray luminosity of X-1 and X-2 was measured as 2.5×10^{40} erg s⁻¹ and 5.8×10^{39} erg s⁻¹, respectively, with the former the highest ever reported for this ULX. The spectrum of X-1 can be explained by a sum of a strong and variable power-law component with a high energy cutoff, and a stable multicolor blackbody with an innermost disk temperature of ~ 0.2 keV. These results suggest that X-1 was in a “very high” state, where the disk emission is strongly Comptonized. The absorber within NGC 1313 toward X-1 is suggested to have a subsolar oxygen abundance. The spectrum of X-2 is best represented, in its

fainter phase, by a multicolor blackbody model with the innermost disk temperature of 1.2–1.3 keV, and becomes flatter as the source becomes brighter. Hence X-2 is interpreted to be in a slim-disk state. These results suggest that the two ULXs have black hole masses of a few tens to a few hundreds solar masses.

Key words: accretion, accretion disks – black hole physics – X-rays: individual (NGC 1313 X-1; NGC 1313 X-2)

1. Introduction

Ultraluminous X-ray sources, or ULXs, are pointlike X-ray sources with bolometric luminosities in excess of 3×10^{39} erg s $^{-1}$. They were first discovered using the Einstein Observatory (for a review of the first decade of ULX discoveries, see Fabbiano 1989), and have often been hypothesized to be massive accreting black-hole binaries (BHBs) because of their high luminosity and time variability. Assuming a simple geometry, an accreting mass of 30–100 M_{\odot} is required so that the observed luminosities do not exceed the Eddington limit, although the firm evidence for this interpretation had been lacking for almost 20 years.

A breakthrough in the study of ULXs was brought about by observations with the ASCA satellite: more than a dozen ULXs were studied spectroscopically in the 0.5–10 keV energy range for the first time (e.g., Okada et al. 1998; Colbert, Mushotzky 1999; Makishima et al. 2000; Mizuno 2000). Spectra of the majority of the ASCA sample have been well modeled by a so-called multi-color disk model (MCD model: Mitsuda et al. 1984). Spectral transitions between the MCD-type state and the power-law type state, often seen in Galactic BHBs, have also been found in some ULXs (La Parola et al. 2001; Kubota et al. 2001a). These spectral characteristics generally reinforce the black hole scenario with masses of 30–100 M_{\odot} for ULXs, although the apparent properties of high disk temperatures (innermost disk temperature T_{in} within the range 1.0–1.8 keV; Makishima et al. 2000) and the change of innermost disk radius (Mizuno et al. 2001) both distinguish them from simple scaled-up versions of stellar-mass BHBs.

In the early 2000s, further advancements were provided from observations made with the Chandra and XMM-Newton Observatories. More than 150 off-nucleus sources, with luminosities exceeding 10^{39} erg s $^{-1}$, have been observed using Chandra, and most of them have been determined to be pointlike at 0.5'' angular resolution (Swartz et al. 2004). Some luminous ULXs were found to be associated with recent star formation activities, suggesting that they originate in young and short-lived systems. High-quality spectra of ~ 30 ULXs, obtained using XMM, were in many cases dominated by a power-law like component, often accompanied by soft excess below 1 keV (e.g., Foschini et al. 2002; Feng, Kaaret 2005; Winter, Mushotzky, Reynolds 2005). This soft component could be interpreted as emission from a cool accretion disk ($T_{\text{in}}=0.1$ –

* present address: Department of Physics, Ehime University, Bunkyo-cho, Matsuyama, Ehime 790-8577

0.3 keV) around a massive black hole of $\sim 10^3 M_\odot$ (e.g., Miller et al. 2003; Miller et al. 2004), although this interpretation is still controversial (e.g., Dewangan et al. 2005; Stobbart et al. 2006; Goad et al. 2006).

Another important clue to the nature of ULXs has been provided through the study of Galactic BHBs. Besides the established two spectral states of BHBs, namely, the low/hard state with a dominant power-law continuum and the high/soft state dominated by an MCD emission (e.g., McClintock, Remillard 2003), two novel states have been identified mainly with RXTE observations of several BHBs (e.g., Kubota et al. 2001b; Kobayashi et al. 2003; Kubota, Makishima 2004). One is a so-called very high state, known since the 1990s (e.g., Miyamoto et al. 1991). As a source gets more luminous than in the soft state and enters this new state, its spectrum again becomes power-law like, presumably due to Comptonization by a hot optically thick plasmas, with the MCD component becoming weaker and sometimes cooler. By re-analyzing the ASCA data of IC 342 source 1, Kubota et al. (2002) showed that the observed power-law type spectrum of this ULX is suggestive of the very high state. The fourth state, characterized by an MCD-like but hotter spectra, is seen when a source is very luminous, close to or even exceeding the Eddington limit. As argued by Kubota, Makishima (2004) through the observation of Galactic BHB XTE J1550–564, this state may correspond to the theoretically predicted "slim disk" solution (e.g., Abramowicz et al. 1988; Szuszkiewicz et al. 1996; Watarai et al. 2000), in which an optically-thick disk with a moderate geometrical thickness is formed and advective cooling becomes important. The slim-disk interpretation successfully explains the high disk temperature and the changes of the disk radius observed from the most luminous class of ULXs (e.g., Mizuno et al. 2001; Ebisawa et al. 2003).

Despite the great progress described above, our understanding of ULXs is still far from satisfactory. In particular, it has been difficult to unambiguously distinguish different modelings of their spectra, and to understand how the spectrum changes as the source varies. In the present paper, we report our new Suzaku results on two ULXs (X-1 and X-2) in the nearby spiral galaxy NGC 1313. We suggest that X-1 was in a state which is very similar to the very high state of Galactic BHBs, while X-2 was in another state which may correspond to the slim disk solution. Our new results also include possible indication of sub-solar oxygen abundance in the X-ray absorption toward X-1.

2. Instrumentation and Observation

The 5th Japanese X-ray satellite Suzaku (Mitsuda et al. 2006) has several important instrumental properties which are suited to ULX studies. The X-ray Imaging Spectrometer (XIS; Koyama et al. 2006), combined with the X-ray Telescope (XRT; Serlemitsos et al. 2006), is our primary observing tool. Among the four XIS cameras, one (XIS1) utilizes a back-side illuminated CCD chip (BI chip), and has an unprecedented sensitivity and energy resolution in the energy band below 1 keV. The other three XIS cameras, with front-side illuminated chips (FI

chips), have an even better energy resolution, together with very low and stable background toward the hardest spectral end. As a result, the XIS plus XRT combination covers a very wide energy range, 0.2–12 keV, with a much flatter response than was achieved with previous missions. This in turn allows us to accurately constrain the continuum shape of ULXs. In addition, the Hard X-ray Detector (HXD; Takahashi et al. 2006; Kokubun et al. 2006) has unprecedented sensitivity in the energy range above 10 keV, and may detect the hard X-ray emission from the brightest ULXs.

NGC 1313 is a nearby face-on, late-type Sb galaxy at a distance of 3.7 Mpc (Tully 1988). Although a more recent estimate by Méndez et al. (2002) gives 4.13 Mpc, we adopt the value by Tully (1988) for consistency with other works on ULXs in this galaxy (e.g., Miller et al. 2003; Dewangan et al. 2005; Stobbart et al. 2006). If 4.13 Mpc is adopted, all the luminosities quoted in the present work increases by 20%. The low Galactic line-of-sight absorption towards NGC 1313 ($N_{\text{H}} = 0.35 \times 10^{21} \text{ cm}^{-2}$) allows us to study low energy spectral properties of sources in it. According to previous X-ray observations of NGC 1313 using the Einstein Observatory and ROSAT (Fabbiano, Trinchieri 1987; Colbert et al. 1995), its X-ray emission is dominated by three extremely luminous pointlike sources of X-ray luminosity $L_{\text{X}} \sim 10^{39} \text{ erg s}^{-1}$ each. One of them is the unusually luminous X-ray supernova, namely SN 1978K. The other two are typical ULXs, which we call X-1 and X-2 after Colbert et al. (1995); the former is located close ($\sim 45''$) to the galaxy nucleus.

The two ULXs have already been studied extensively with ASCA and XMM-Newton (e.g., Makishima et al. 2000; Mizuno et al. 2001; Miller et al. 2003; Dewangan et al. 2005; Stobbart et al. 2006; Feng, Kaaret 2006). ASCA observations found moderate amplitude long-term variability of these ULXs. While the spectral behavior of X-1 was rather complex, the ASCA spectrum of X-2 was represented by a hot (1.0–1.5 keV) MCD model (Mizuno 2000; Mizuno et al. 2001). The XMM spectra of both ULXs in 2000 can be represented by a power-law with soft excess, which Miller et al. (2003) interpreted as MCD emission from a cool accretion disk around a very massive ($\sim 1000 M_{\odot}$) BH. Optical observations of X-2 indicate that the source is a high-mass X-ray binary system (Zampieri et al. 2004; Mucciarelli et al. 2005).

We conducted a Suzaku observation of NGC 1313 on 2005 October 15, with the XRT optical axis aimed at the middle point between X-1 and X-2. The data were screened based on the following standard criteria: a) The time elapsed after a passage through the South Atlantic Anomaly is longer than 256 seconds, b) The object is at least 5° and 20° above the rim of the Earth during night and day, respectively, and c) The geomagnetic cutoff rigidity is greater than 6 GV. After these data screenings, the net exposure with the XIS became 27.8 ks. The resulting XIS image of the galaxy is shown in figure 1. The spectrum of the HXD, after subtracting the instrumental background model provided by the instrument team, is consistent with that of the cosmic X-ray background (Boldt 1987), and no significant hard X-ray emission above 10 keV

was detected.

3. Data Analysis

3.1. Light Curves of two ULXs

The 0.4–10 keV light curves of NGC1313 X-1 and X-2, extracted from the circular regions of $3'$ radius, are shown in figure 2. Thus, the two ULXs both varied by $\sim 50\%$, with a flux increase in X-1 and a decrease in X-2. The variations are intrinsic to the sources rather than being instrumental artifacts (e.g., vignetting of the mirror), since we used the data after the satellite position was well stabilized, and because both objects were placed rather close ($\sim 3.5'$) to the optical axis of the telescope compared to the XIS field-of-view ($18' \times 18'$).

To investigate the change of spectral shapes in a model independent way, we subtracted background extracted from a source free region of the same observation, and calculated the ratio of the spectrum of the fainter phase to that of the brighter phase. The observed ratios, shown in figure 3, reveal intensity-correlated spectral changes in both ULXs. In X-1, the ratio stays at ~ 1 below 1 keV, and decreases toward higher energies, reaching ~ 0.6 at 3 keV and then flattening. The positive correlation between the intensity and spectral hardness, observed from X-1 in this particular observation, is in the opposite sense as found on other occasions (e.g., Dewangan et al. 2005; Feng, Kaaret 2006). The X-2 spectrum softens as the source gets dimmer, implying also a positive intensity vs. hardness correlation, but the spectral change is particularly prominent in energies above ~ 3 keV.

In the following sections, we first analyze the time-averaged spectra to grasp rough spectral information (§ 3.2), and then study the spectral variability in detail (§ 3.3).

3.2. Time-averaged Spectra

We first calculated spectral ratios of the two ULXs to the Crab Nebula (Crab ratio). Since the Crab Nebula is known to have a stable, simple power-law X-ray spectrum of the photon index $\Gamma \sim 2.1$ (Toor, Seward 1974), the Crab ratios can be used to roughly examine spectral shapes of various X-ray sources in the form close to νF_ν representation, without using a detector response. As shown in figure 4, the X-1 spectrum has a power-law like shape up to 3 keV, and then falls off above 5 keV. The X-2 spectrum shows a similar shape, but is more convex than that of X-1. Thus, neither spectrum can be well modeled by a single power-law.

We then fitted the time-averaged spectra by xspec of version 11.3 using the response matrix files as of 2006 February 13, and auxiliary response files generated by the program xissimarfgen as of 2006 April 24. Since the two ULXs exhibited clear spectral changes during the observation, here we aim at roughly evaluating spectral properties rather than quantifying the spectral parameters. We employed the MCD plus power-law model (hereafter called "MCD+PL" model), a standard model widely used to describe the spectra of BHBs and ULXs. The data from the three FI cameras were summed together to improve the statis-

tics. Contamination on the XIS by out-gassing from the satellite (Koyama et al. 2006) and the consequent decrease in the low-energy efficiency were taken into account using the xispcwab model ¹ developed by the XIS team; this empirically models the positional dependence and time evolution of the contaminant thickness of each XIS sensor based on calibration observations. Two free parameters of the model, namely the date of observation and the target offset angle from the XIS nominal position, were fixed at 63 and 3.5, respectively; the model gave a column density of $1.0\text{--}2.9 \times 10^{18} \text{ cm}^{-2}$ and $0.18\text{--}0.48 \times 10^{18} \text{ cm}^{-2}$ for carbon and oxygen in the contaminant, respectively. The line-of-sight absorption outside the satellite was taken into account using the “wabs” model (Morrison, McCammon 1983), with hydrogen column density as a free parameter. Since a small gain jump at the Si K edge is not yet properly handled in the current pipeline processing, data with PI channels 500–504 (corresponding to 1.82–1.84 keV) are ignored in the fitting.

As shown by figure 5, the model approximately reproduces the data, although the fit is rather poor with $\chi^2/\nu = 442.6/282$, mainly because of residuals in the 0.4–0.6 keV band and around 2 keV. Since the shape of the residuals around 2 keV is different between the FI and BI spectra, this is likely to be instrumental due to calibration uncertainties. We therefore exclude data in the 1.5–2.3 keV band (which covers the 1.82–1.84 keV range already excluded) in the following analysis of the X-1 spectrum. The low-energy residuals are prominent below the neutral O-edge absorption, and is suggestive of an incorrect amount of oxygen in the spectral model. We therefore exclude, for the moment, the X-1 data below 0.6 keV as well, and investigate this issue in § 3.4. Neglecting the data in these two energy regions gives a marginally acceptable fit to the X-1 spectrum with $\chi^2/\nu = 256.9/218$. The X-2 spectrum, in contrast, is reproduced successfully by the MCD+PL model with $\chi^2/\nu = 152.2/142$, probably because of the limited photon statistics. We thus utilize the full energy band of the Suzaku XRT+XIS (except the 1.82–1.84 keV range) in the following spectral analysis of X-2.

The best fit model parameters describing the time averaged X-1 and X-2 spectra are tabulated in table 1, and contributions of the individual model components are shown in the insets to figure 5. The power-law component and the MCD component contribute almost equally to the X-1 spectrum, whereas the MCD component dominates the X-2 spectrum. These properties agree with the inference from the Crab ratio (figure 4). Assuming the source distance of 3.7 Mpc (Tully 1988) and isotropic radiation, the 0.4–10 keV source luminosity is $2.5 \times 10^{40} \text{ erg s}^{-1}$ and $5.8 \times 10^{39} \text{ erg s}^{-1}$ for X-1 and X-2, respectively, after correction for the absorption inside and outside the spacecraft. Even allowing for possible calibration uncertainties by $\sim 10\%$, the flux of X-1 is the highest among those ever reported for this source including all archival XMM-Newton data available as of June 2006, as we confirmed through our own analysis; more than a factor of 4 higher than that of the XMM-Newton 2000 observation. The flux of X-2 is between those of the 1993 and 1995 ASCA observations, and a factor of 3 higher than that measured in

¹ <http://heasarc.gsfc.nasa.gov/docs/xanadu/xspec/models/xisabs.html>

the XMM-Newton observation in 2000 (Mizuno et al. 2001; Miller et al. 2003).

3.3. Spectral Variability of Each Source

To quantify the spectral changes (figure 3) associated with the intensity variations, we then divided the data into two time regions shown in figure 2, and derived “brighter phase” and “fainter phase” spectra from the two sources. We then fitted them with several models widely used to represent the spectra of ULXs: the MCD+PL model, so called p -free disk model, and the MCD plus cutoff power-law model (hereafter MCD+cutoff-PL). The MCD+PL model is the most commonly used description of BHB spectra, mainly those in the soft state. The p -free disk model is a modified MCD model, where the disk temperature profile as a function of radius r is given as $T(r) = T_{\text{in}}(r/r_{\text{in}})^{-p}$ with p being a positive free parameter. This model was originally developed by Mineshige et al. (1994) to validate the standard accretion disk prediction on the temperature profile ($p = 0.75$). The model was later utilized to represent the spectra of BHBs and ULXs when the objects are thought to be in the slim disk state (e.g., Kubota, Makishima 2004), since the spectrum emergent from a slim disk is theoretically predicted to become flatter, and be approximated by the p -free disk model with p decreasing to ~ 0.5 (Watarai et al. 2000). A power-law type hard spectrum with soft excess below 1 keV has been widely observed in ULXs including those in NGC 1313 (Miller et al. 2003). Since the apparently power-law like continuum often exhibits, in close inspection, a high-energy turn over (e.g., Kubota et al. 2002; Dewangan et al. 2005; Stobbart et al. 2006), we also employed the MCD+cutoff-PL model in which the MCD component represents the excess in the soft band and the cutoff-PL represents the curved spectrum in the high energy band. The role of the MCD component in this model is different from that in the first one (MCD+PL), in which the MCD component has a high temperature and represent the high-energy spectral curvature.

All these three models are moderately successful on both the fainter-phase and brighter-phase spectra of X-1, yielding the best fit parameters as summarized in table 2. The MCD and p -free disk models allow us to evaluate the innermost disk radius R_{in} . After Makishima et al. (2000), we calculated this parameter as $R_{\text{in}} = \xi \kappa^2 \sqrt{N / \cos i}$ ($D/10$ kpc), where N is the model normalization, i is the disk inclination angle, and D is the distance to the source; $\xi = 0.41$ and $\kappa = 1.7$ are correction factors described in Kubota et al. (1998) and Shimura, Takahara (1995). The best-fit spectrum of each phase is given in figure 6. Physical meanings of the obtained fits are discussed in § 4.1.

We obtained similar results on the brighter-phase X-2 spectrum: the three model are all moderately successful, with a rather small difference in their fit goodness (table 2). The fainter-phase spectra of X-2 were reproduced by a single MCD model, and adding a power-law component with $\Gamma=1.0$ – 2.5 did not improve the fit significantly (less than 90% confidence using the F -test). In table 2, we hence give only the single-MCD fit result for the fainter-phase X-2 spectrum. The spectra of X-2 in its fainter and brighter phases are shown in figure 7 together

with the best-fit models (see § 4.2 for the discussion of physical meanings of the model fits).

3.4. *Residuals at Low Energies*

Finally, we revisit the residuals seen at low energies in the X-1 spectrum, particularly around the oxygen absorption edge (at 0.53 keV in figure 5). These residuals suggest that the model is over-predicting the edge depth. Then, a likely origin is an overestimation of oxygen column density in the XIS contamination model, or an incorrect modeling of oxygen abundance in absorbing materials along the line of sight to the source.

To better estimate the oxygen column density in the overall absorber, we followed the procedure of Cropper et al. (2004), and decomposed the absorption into the following two factors. One is the line-of-sight Galactic absorption, represented by a “wabs” model with solar abundance ratios, of which the column density is fixed at $N_{\text{H}} = 0.35 \times 10^{21} \text{ cm}^{-2}$. The other is absorption inside NGC 1313 (plus errors in the XIS contamination modeling), expressed by a “tbvarabs” absorption model (Wilms, Allen, McCray 2000) in which abundances of individual elements can be varied. We selected the MCD+cutoff-PL model to represent the continuum, because it can reproduce the brighter phase spectrum with the smallest χ^2/ν among the three model fits. The elemental abundances refer to Anders, Ebihara (1982), which are close to those employed in the “wabs” model. We refitted the data, leaving the oxygen abundance in the tbvarabs model to vary freely, but fixing other elemental abundances at the solar values. Indeed, the fit was improved ($\Delta\chi^2 = -50.3$) by lowering the oxygen abundance to $0.51^{+0.11}_{-0.05}$ solar. According to an F -test, this improvement is significant at the 99% confidence limit.

We further allowed the FI and BI data to have independent absorption parameters, to see if there are any possible instrumental uncertainty. Then, the FI and BI data gave consistent column densities of the second absorption factor as $N_{\text{H}} = (3.3 \pm 0.3) \times 10^{21} \text{ cm}^{-2}$ and $N_{\text{H}} = (2.8 \pm 0.2) \times 10^{21} \text{ cm}^{-2}$, respectively, whereas they somewhat disagreed on the circum-source oxygen abundance; 0.31 ± 0.10 solar (FI) and 0.68 ± 0.13 solar (BI). Since the FI sensors have lower soft X-ray efficiency than the BI sensor, and may suffer from larger calibration uncertainties, we adopt the result by the BI data, which still implies the subsolar oxygen abundance.

If we adopt the 0.68-solar oxygen abundance in the tbvarabs model, the intervening oxygen column density decreases by $0.67 \times 10^{18} \text{ cm}^{-2}$ from that implied by the one-solar abundance modeling. This decrement is significantly larger than the oxygen column density contained in the BI sensor contaminant, namely $0.21 \times 10^{18} \text{ cm}^{-2}$. Therefore, the required reduction in the oxygen column density cannot be attributed to any uncertainty in the modeling of chemical composition and/or thickness of the XIS contaminant. Instead, we infer that the absorber within NGC 1313 toward X-1 has a subsolar oxygen abundance.

We performed the same analysis on X-2. Namely, we refitted the spectrum by allowing the oxygen abundance in the tbvarabs model to vary freely. Due to the limited photon statistics,

however, the oxygen abundance in this absorption model was only poorly constrained, with an upper limit of ≤ 1.01 solar. Thus, the X-2 data are consistent with the absorber in NGC 1313 having a sub-solar oxygen abundance, but do not require it.

4. Discussion

In the Suzaku observation of NGC 1313 spanning a gross time interval of 90 ks (but the net exposure being 28 ks), we detected gradual intensity changes by $\sim 50\%$ from the two ULXs, X-1 and X-2. When time averaged, X-1 exhibited a 0.4–10 keV luminosity of 2.5×10^{40} erg s $^{-1}$, which is the highest value ever reported for this source, while X-2 showed 5.8×10^{39} erg s $^{-1}$. Thanks to the excellent performance of the Suzaku XIS, we obtained high-quality spectra from both ULXs, and revealed their intensity-correlated spectral changes. The high flux of X-1 also allowed us to obtain evidence of a subsolar oxygen abundance in the absorption toward it. Below we examine spectral states of the two ULXs, and discuss environment of the NGC 1313 X-1 system.

4.1. Spectral State of X-1

In the fainter phase, NGC 1313 X-1 exhibited a more or less straight continuum, with the power-law component in the MCD+PL fit contributing more than 80% (see table 2). In the brighter phase, in contrast, the spectrum was much more convex (top panel of figure 3). In both phases, however, the three models tried here all gave similar χ^2/ν . Therefore, the fit goodness alone cannot tell which model is most appropriate in describing the spectra of X-1. Accordingly, below we examine each model for its physical consistency, utilizing in particular the variation as a key probe.

The MCD+PL model reproduces the data well in both brighter and fainter phases, and the inferred disk temperature ($T_{\text{in}}=1.3\text{--}1.6$ keV) is similar to those seen in high-temperature ULXs. However, the contribution of the MCD component is only 20–50%; this is much smaller than is seen in high-temperature ULXs where the MCD component dominates their X-ray spectra. This leads to a small inferred disk radius (~ 100 km), and as a consequence, the implied Schwarzschild black-hole mass (with R_{in} identified with three times the Schwarzschild radius R_{s}) becomes more than an order of magnitude less than that derived employing the observed luminosity and consistency with the Eddington limit. In addition, the dominance of the PL component at low energies (figure 5) would cause difficulties in understanding the spectrum in an analogy to the BHB’s soft state, as discussed, e.g., by Roberts et al. (2005). Therefore, the MCD+PL modeling fails to give a satisfactory physical interpretation.

Although we employed the p -free disk model to examine the slim-disk interpretation, the derived results appear to be self-contradictory to this view. It yields somewhat worst χ^2/ν for both the fainter and brighter phase spectra, together with unusually high innermost disk temperature, T_{in} , exceeding 2 keV. In addition, the p -free model fits imply that the temperature

profile coefficient p increases and T_{in} decreases as the source gets brighter; these dependences are both opposite to theoretical predictions by the slim disk model, and disagree with previous observations of BHBs/ULXs which are thought to be in the slim disk state (e.g., Mizuno et al. 2001; Kubota, Makishima 2004). Therefore, X-1 is not likely to be in the slim disk state.

As shown in figure 3, the X-1 spectrum below 1 keV stayed nearly constant, and only the hard part of the spectrum varied. This behavior is most successfully represented by the third modeling, namely MCD+cutoff-PL, making it promising. In fact, the MCD component in this fit is consistent with being constant (table 2, figure 6), and the variation in the cutoff-PL component alone can account for the intensity and spectral changes. The cutoff-PL component represents a power-law like, but slightly convex, continuum shape. Such a slightly convex hard continuum has been recently observed from many apparently PL-like ULXs, e.g.; IC 342 X-1 by Kubota et al. (2002); Holmberg IX X-1 by Dewangan, Griffith, Rao (2006); Holmberg II X-1 by Goad et al. (2006); many of the sample of 13 ULXs studied by Stobbart et al. (2006); 4 of the objects studied by Winter, Mushotzky, Reynolds (2005); and NGC 1313 X-1 itself by Dewangan et al. (2005). Since these ULXs often exhibit a soft spectral excess simultaneously, the “soft excess plus power-law with high energy cutoff” spectral shape is considered rather common among a certain class of luminous ULXs. In addition, the same cutoff-PL modeling was successfully employed by Murashima et al. (2005) to explain the variable soft X-ray excess of the narrow-line Syfert 1 galaxy Ton S180. As the cutoff-PL model generally approximates the process of unsaturated Comptonization, the slightly convex continua from these high-accretion-rate black holes may be interpreted as a result of Comptonization of some soft photons by hot (in this case, a few keV) thermal electrons, which presumably form a disk corona.

Then, how can we interpret the MCD parameters derived from the MCD+cutoff-PL fit? The MCD component is considered to be emitted by a cool disk with a temperature of ~ 0.2 keV. The derived face-value radius of $R_{\text{in}} \sim 4000$ km (table 2), if identified with $3R_{\text{s}}$, implies a black hole of several hundred solar masses. However, the luminosity attributed to the MCD component is only a few times 10^{39} erg s $^{-1}$ ($\sim 10\%$ of the total luminosity; table 2), which is an order of magnitude lower than the corresponding Eddington limit. This appears to contradict to our basic assumption that ULXs are under high accretion rates. Furthermore, the value of R_{in} we obtained is 3–4 times smaller than that measured by Miller et al. (2003) from the same source in 2000 using XMM-Newton (although the errors of the Suzaku measurement are quite large due to the strong cutoff-PL component). Similarly, Dewangan et al. (2005) analyzed three XMM-Newton observations of X-1, and reported lack of the luminosity-correlated temperature changes in the soft component which would take place if the emission is emerging from a standard accretion disk. These pieces of evidence, taken altogether, suggests that the optically-thick disk, if present, has a much larger inner radius than $3R_{\text{s}}$, or that the disk temperature is unusually low for the accretion rate.

A plausible explanation of such a cool disk has been obtained through the study of the

Galactic BHB, XTE J1550–564, in the very high state (Kubota, Done 2004; Done, Kubota 2005). In this state, a large fraction of the gravitational energy is thought to be dissipated from a hot corona rather than from the optically-thick disk. Consequently, it is considered that the accretion disk is truncated at a certain large radius if the disk and corona are energetically independent (Kubota, Done 2004), or that the disk becomes much cooler if it is strongly coupled to the corona which takes up most of the gravitational energy release (Done, Kubota 2005). Then, the successful MCD+cutoff-PL fit to the X-1 spectra leads to a view that the source is in the very high state, hosting a cool disk and a hot Comptonizing corona. The same very-high-state interpretation, but invoking lower accretion rates, may also apply to the X-1 spectra obtained with XMM-Newton by Miller et al. (2003), Dewangan et al. (2005), and Feng, Kaaret (2006), when the source was fainter than in the present Suzaku observation.

Since the cool disk can no longer be regarded as extending down to $3R_s$, we cannot utilize the MCD parameters in estimating the black-hole mass. Instead, a relatively robust estimate on the BH mass may be obtained from the source luminosity. The bolometric luminosity inferred from the MCD+cutoff-PL fit to the Suzaku brighter-phase data of X-1 is $3.3 \times 10^{40} \text{ erg s}^{-1}$, requiring a BH mass of $\sim 200 M_\odot$ to satisfy the Eddington limit. Even if we allow a super-Eddington condition by a factor of 3, a mass of $70 M_\odot$ is necessary, which has never been observed in Galactic or Magellanic BHBs.

4.2. Spectral State of X-2

The fainter phase spectrum of X-2 is rather convex, and is successfully reproduced by a single MCD model. Therefore, X-2 in this phase may be regarded as a hot-MCD type ULX, just as it was so in the two ASCA observations (Makishima et al. 2000; Mizuno et al. 2001). When plotted on the temperature-luminosity diagram of ULXs (figure 4 of Makishima et al. 2000), the present fainter-phase data point of X-2, after the correction for the adopted distance to the source, just falls on the line connecting the two ASCA data points of this source. Since these hot-MCD type ULXs are successfully interpreted as residing in the slim-disk state (§ 1), it is natural to consider, as a working hypothesis, that X-2 is also in the slim-disk state at least during its fainter phase.

The brighter-phase Suzaku spectrum of X-2 has a flatter shape as shown by figure 3. If we force a single MCD model to fit this spectrum, we obtain $T_{\text{in}} = 1.50 \pm 0.04 \text{ keV}$ and $R_{\text{in}} = 80 \pm 4 \text{ km}$, even though the fit is relatively poor ($\chi^2/\nu = 172.0/144$). With these values, the brighter-phase data point falls close to the ASCA 1993 data point on the same temperature-luminosity diagram. Thus, the four data points of X-2, two from ASCA and two from Suzaku, define a common locus on the diagram, which is characterized by $T_{\text{in}} \propto R_{\text{in}}^{-1}$ (or equivalently, $L_{\text{disk}} \propto T_{\text{in}}^2$). This relation is just what is predicted by the slim disk model (Watarai et al. 2000). A more solid evidence for the slim disk is provided by the fact that the p -free disk model fit to the brighter phase spectrum gives the temperature coefficient as $p \sim 0.63$, which is significantly

smaller than that of the standard disk ($p = 0.75$), and is consistent with what is predicted for a slim disk (Watarai et al. 2000). From these arguments, we conclude that X-2 was in the slim-disk state throughout the present observation. Although alternative interpretations based on the other two modelings cannot be ruled out, the p -free fit to the brighter phase data provides a most natural extension to the successful MCD fit to the fainter phase spectrum.

If we assume that X-2 is shining close to the Eddington limit, the observed luminosity requires a black-hole mass of $\sim 50 M_\odot$. The value of $R_{\text{in}} \sim 100$ km, estimated using a simple MCD model, appears by a factor of ~ 5 smaller than that inferred from the BH mass. This could be due either to a high BH spin parameter, and/or to the characteristics of slim disks, as argued originally by Makishima et al. (2000) and Mizuno et al. (2001), respectively.

In the XMM-Newton observation conducted in 2000 (Miller et al. 2003), X-2 was a factor of 2 less luminous than in the fainter phase observed with Suzaku. The XMM-Newton data were reproduced by a power-law model with $\Gamma = 1.8$ plus a soft excess emission, suggesting that the source was in the very high state. This is reasonable, because a few Galactic BHBs show slightly higher luminosities (and probably much higher accretion rates) in the slim-disk state than they are in the very high state (e.g., Kubota, Makishima 2004).

In closing this subsection, let us briefly compare the two ULXs. When time averaged, X-1 that is presumably in the very high state is about 4 times more luminous, than X-2 that is interpreted to be in the slim-disk state. However, we cannot assign a higher *normalized* luminosity $\eta \equiv L_X/L_{\text{Ed}}$ (with L_{Ed} being the Eddington limit) to X-1, since the slim-disk state is thought to appear at a higher, or at least comparable, value of η as compared to the very high state (Kubota, Makishima 2004). We may hence conservatively assume that the two ULX have comparable values of η . Then, neglecting any effect due to possible differences in their inclination, X-1 is inferred to have (at least) 4 times higher Eddington luminosity, and hence 4 times higher mass, than X-2. Then, even employing an extreme assumption that X-2 has a rather ordinary stellar mass, e.g., $\sim 10 M_\odot$ that requires $\eta \sim 4$, X-1 is inferred to have $\sim 40 M_\odot$, indicating that ULXs have a rather broad mass spectrum. Of course, a more reasonable view invoking $\eta \sim 1$ would be to assign $\sim 200 M_\odot$ to X-1 (§ 4.1) and $\sim 50 M_\odot$ to X-2.

4.3. Oxygen Abundance

The present Suzaku observation has for the first time provided evidence that the oxygen abundance in the absorption intrinsic to X-1 is significantly lower than the solar value, at 0.68 ± 0.13 relative to that given by Anders, Ebihara (1982). This translates to an oxygen to hydrogen number ratio of $\text{O}/\text{H} = (5.0 \pm 1.0) \times 10^{-4}$. This value is consistent with that of the interstellar medium (ISM) in our Galaxy, according to a recent compilation by Wilms, Allen, McCray (2000). It is thus likely that the oxygen abundance in the ISM is subsolar in NGC 1313 as well as in the Milky Way. We also note that recent measurements of the solar oxygen abundance are reconciled with the ISM oxygen abundance, as discussed by Baumgartner, Mushotzky (2006).

5. Summary

Using the Suzaku XIS, we observed the two ULXs, X-1 and X-2, in NGC 1313. Both sources varied by about 50% in 90 ks, and showed intensity-correlated spectral changes. The brighter source, X-1, exhibited the highest luminosity, 2.5×10^{40} erg s⁻¹ (0.4–10 keV), ever recorded from this source. The intensity and spectral variations of X-1 are both ascribed to a strong power-law like component with a mild high energy curvature, while about 10% of the flux is carried by a stable soft component which can be modeled by a cool (~ 0.2 keV) disk emission. These properties suggest that the source was in the “very high” state, wherein the emission is dominated by photons Comptonization in a hot corona, whereas the optically-thick disk is truncated at a large radii or cooled off as the accretion energy is taken up by the corona. The observed properties of X-2 are consistently interpreted by presuming that it was in the slim disk state. The higher luminosity of X-1 than X-2 suggests that the black hole in X-1 is at least ~ 4 times as massive as that in X-2.

We would like to thank N. White and Suzaku managers for valuable comments. We are also grateful to K. Hayashida for helpful discussions. We also thank all the Suzaku team members for their dedicated support of the satellite operation and calibration. This work was partially supported by the Grant-in-Aid for Scientific Research of Japan Society for the Promotion of Science (No. 18740154).

Table 1. Time-averaged ULX spectra fitted with the MCD+PL model

	N_{H}^*	T_{in}	f_{disk}^\dagger	Γ	f_{pow}^\ddagger	L_{X}^\S	χ^2/ν
source	(10^{21} cm^{-2})	(keV)					
X-1	2.1 ± 0.3	1.60 ± 0.15	6.13	$2.08^{+0.17}_{-0.21}$	6.27	25.4	256.9/218
X-2	$1.1^{+0.7}_{-0.2}$	1.29 ± 0.08	2.42	$1.17(\leq 1.89)$	0.83	5.8	152.2/142

Notes. Errors are calculated for 90% confidence for one interesting parameter ($\Delta\chi^2 = 2.7$)

* Hydrogen column density of the photoelectric absorption

[†] observed 0.4–10 keV flux of the MCD component in units of $10^{-12} \text{ erg s}^{-1} \text{ cm}^{-2}$

[‡] observed 0.4–10 keV flux of the PL component in units of $10^{-12} \text{ erg s}^{-1} \text{ cm}^{-2}$

[§] X-ray luminosity in 0.4–10 keV in units of $10^{39} \text{ erg s}^{-1}$ after removing the absorption

^{||} Data below 0.6 keV and in 1.5–2.3 keV band are not used for the spectral fitting.

Table 2. Fits to time-sorted spectra with errors for 90% confidence for one interesting parameter

model	N_{H}	T_{in}	R_{in}	Γ or p	E_{c}	f_{disk}^*	f_{pow}^\dagger	χ^2/ν
	(10^{21} cm^{-2})	(keV)	($\frac{1}{\cos i} \text{ km}$)		(keV)			
X-1 [‡]								
fainter phase								
MCD+PL	2.4 ± 0.7	$1.30^{+0.65}_{-0.36}$	89^{+106}_{-54}	$2.09^{+0.41}_{-0.26}$		2.32	10.37	82.5/94
p -free	2.3 ± 0.2	$2.69^{+0.88}_{-0.38}$	$21(\leq 31)$	0.514 ± 0.014		12.47		83.9/95
MCD+cutoff-PL	$3.0^{+2.1}_{-1.5}$	$0.20(\leq 0.41)$	$4500(\leq 25000)$	$1.59^{+0.33}_{-0.60}$	$6.04^{+6.84}_{-2.27}$	1.92	11.72	82.1/93
brighter phase								
MCD+PL	2.0 ± 0.4	$1.63^{+0.13}_{-0.17}$	107^{+23}_{-11}	2.03 ± 0.24		8.31	8.00	240.4/218
p -free	1.8 ± 0.2	2.09 ± 0.10	60 ± 7	0.595 ± 0.012		15.58		243.4/219
MCD+cutoff-PL	$2.3^{+0.5}_{-0.8}$	$0.21^{+0.13}_{-0.03}$	3800^{+6700}_{-3200}	0.89 ± 0.20	$3.41^{+0.57}_{-0.40}$	1.48	15.13	237.9/217
X-2								
fainter phase								
MCD	0.9 ± 0.3	1.24 ± 0.05	96 ± 9			2.28		71.2/76
brighter phase								
MCD+PL	$1.6^{+0.7}_{-0.4}$	$1.39^{+0.24}_{-0.14}$	80^{+30}_{-20}	$1.62^{+0.58}_{-1.09}$		2.59	1.61	148.9/142
p -free	1.7 ± 0.4	1.86 ± 0.15	43^{+12}_{-9}	$0.627^{+0.036}_{-0.026}$		4.20		150.8/143
MCD+cutoff-PL	2.1 ± 0.9	$0.24(\leq 0.57)$	$1300(\leq 4600)$	$0.59^{+0.27}_{-0.41}$	$2.61^{+0.58}_{-0.47}$	0.36	4.01	147.6/141

* observed 0.4–10 keV flux of the MCD or the p -free disk component in unit of $10^{-12} \text{ erg s}^{-1} \text{ cm}^{-2}$

[†] observed 0.4–10 keV flux of the cutoff PL component in unit of $10^{-12} \text{ erg s}^{-1} \text{ cm}^{-2}$

[‡] Data below 0.6 keV and within the range 1.5–2.3 keV are not used for the spectral fitting.

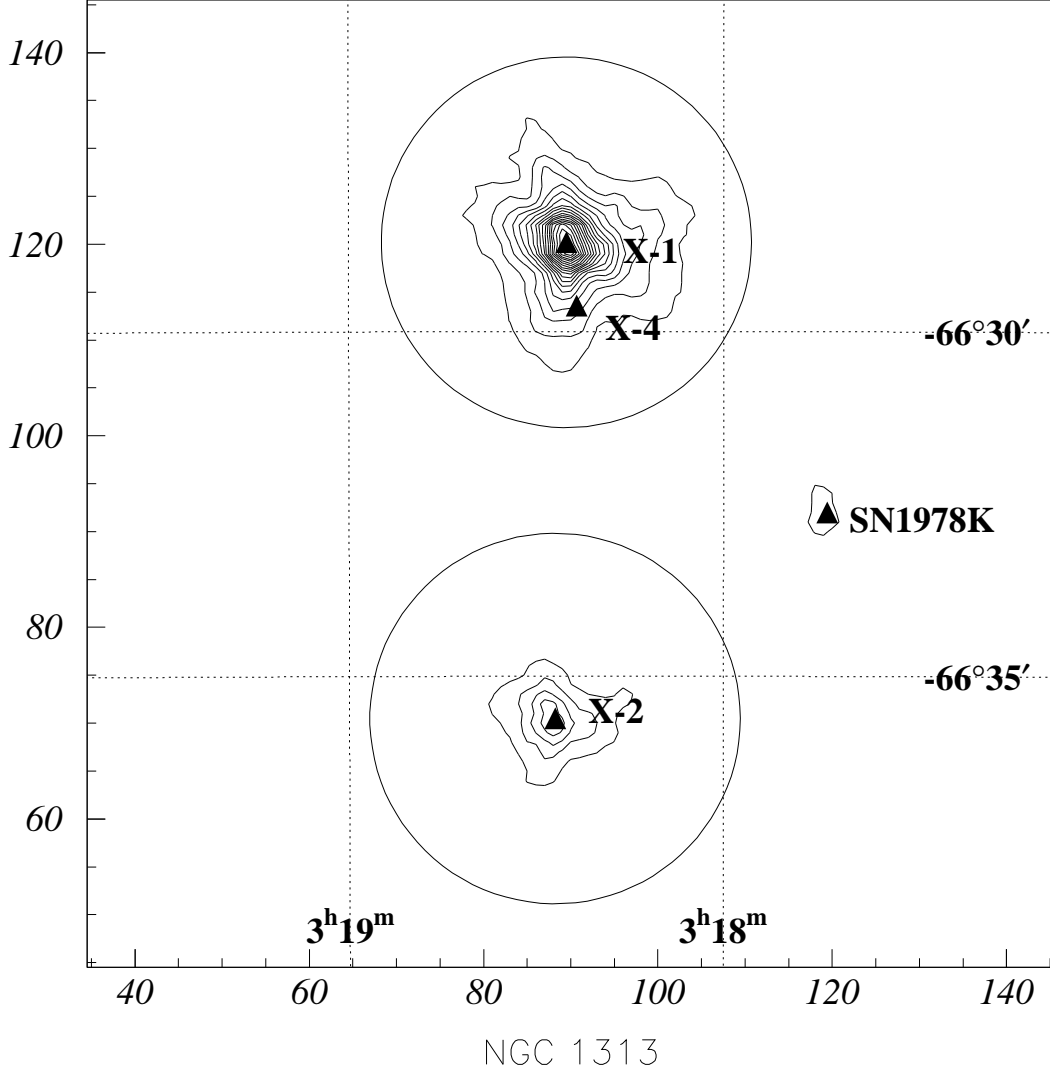


Fig. 1. An XIS0 image of the NGC 1313 region in the 0.4–10 keV band, where we can see X-1, X-2 and SN 1978K as local peaks in the X-ray contours. The image was smoothed using a gaussian distribution with $\sigma = 0.1$. Triangles indicate the positions of strong X-ray sources detected in the ROSAT HRI observation (Schlegel et al. 2000), shifted by 0.65 which is within the pointing accuracy of the Suzaku satellite. Also shown are the accumulation regions for source spectra. Note that source names are after Colbert et al. (1995).

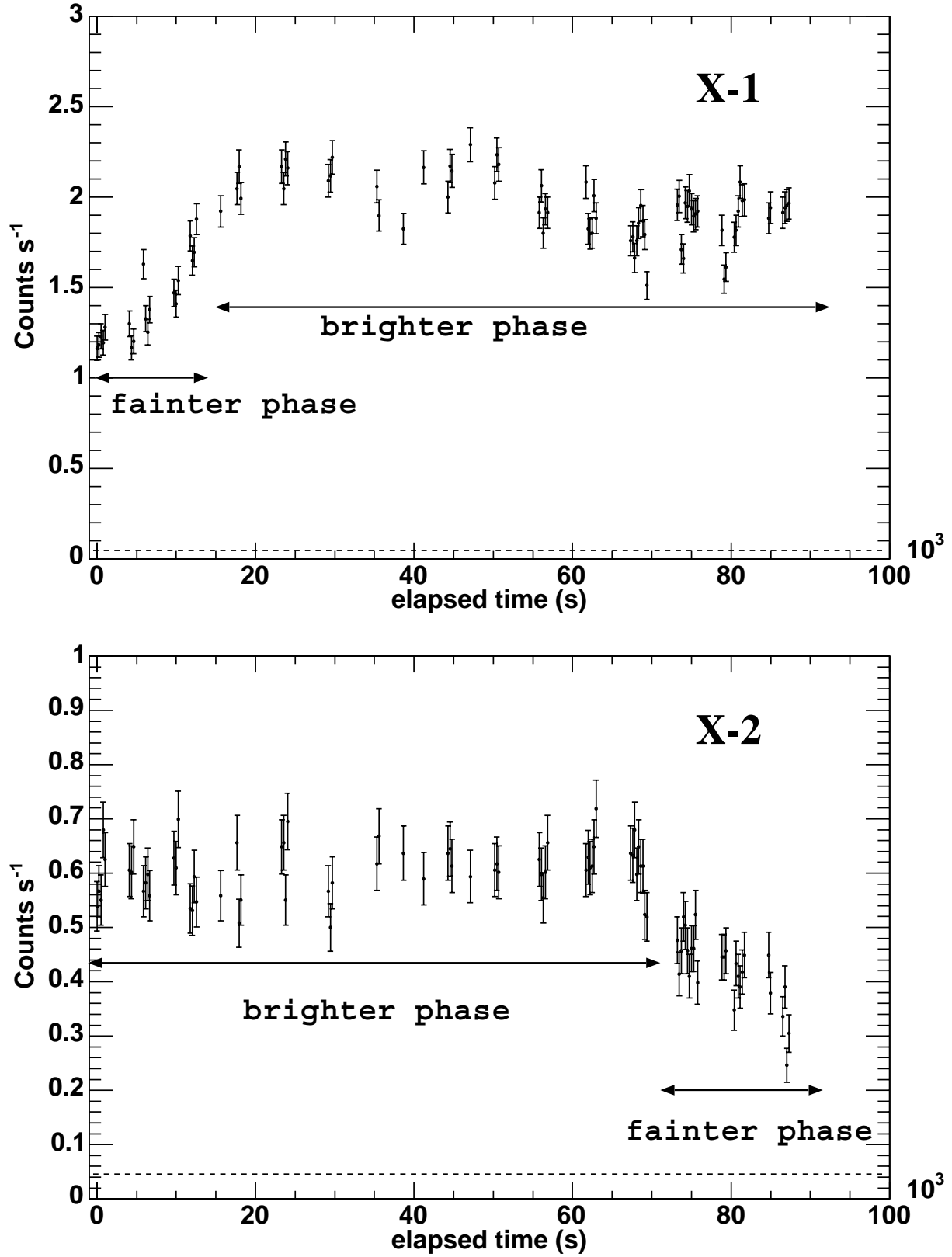


Fig. 2. Suzaku FI light curves for X-1 (top panel) and X-2 (bottom panel) in the 0.4–10 keV energy range with 256 s binning. Background is included and the background level is indicated by dotted lines. Also shown are the time intervals used to study the short-term spectral variability.

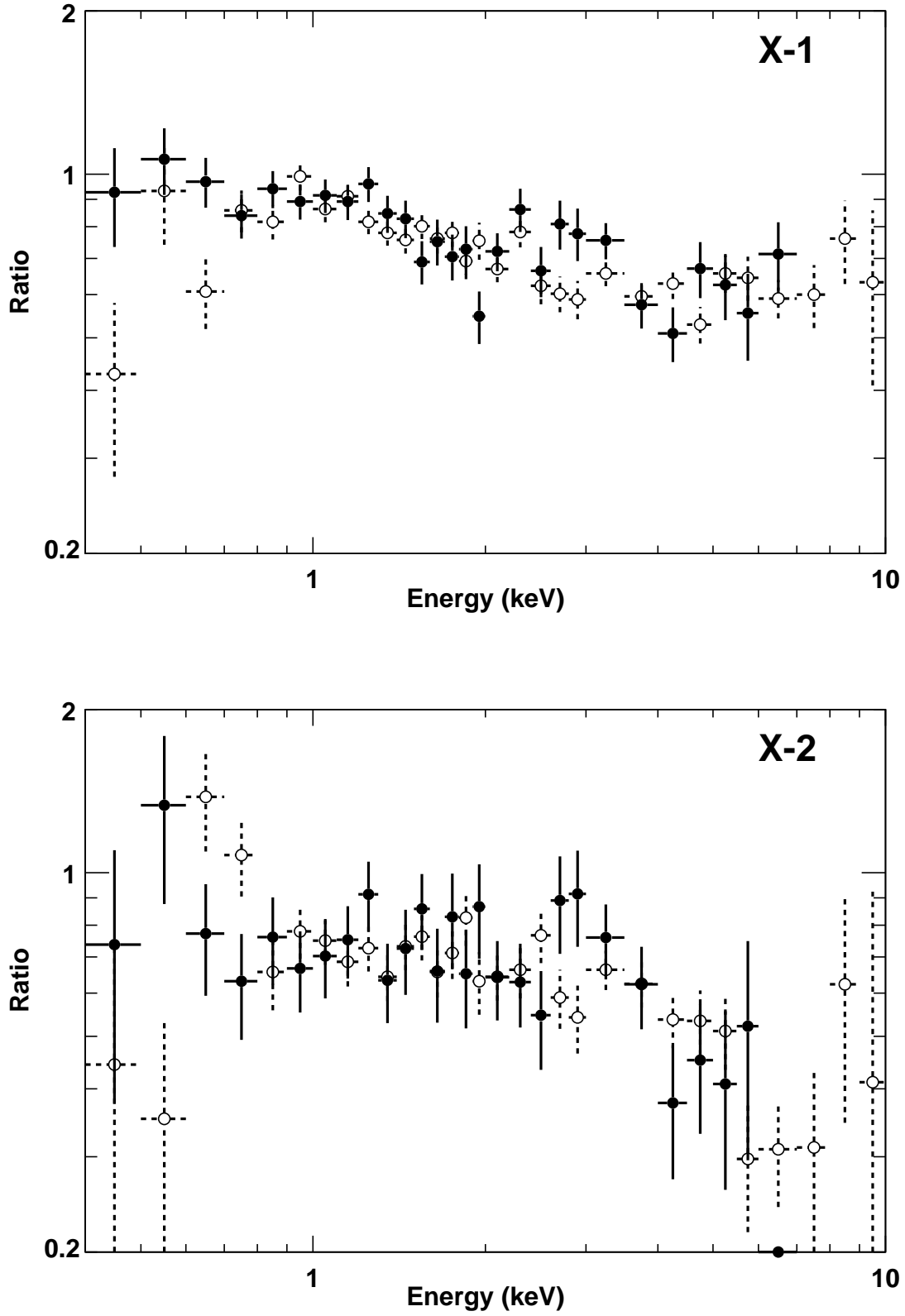


Fig. 3. Spectral ratios of the fainter phase to the brighter phase for X-1 (top panel) and X-2 (bottom panel), calculated after subtracting the background. The ratio of BI and FI data are given as filled circles and open circles, respectively.

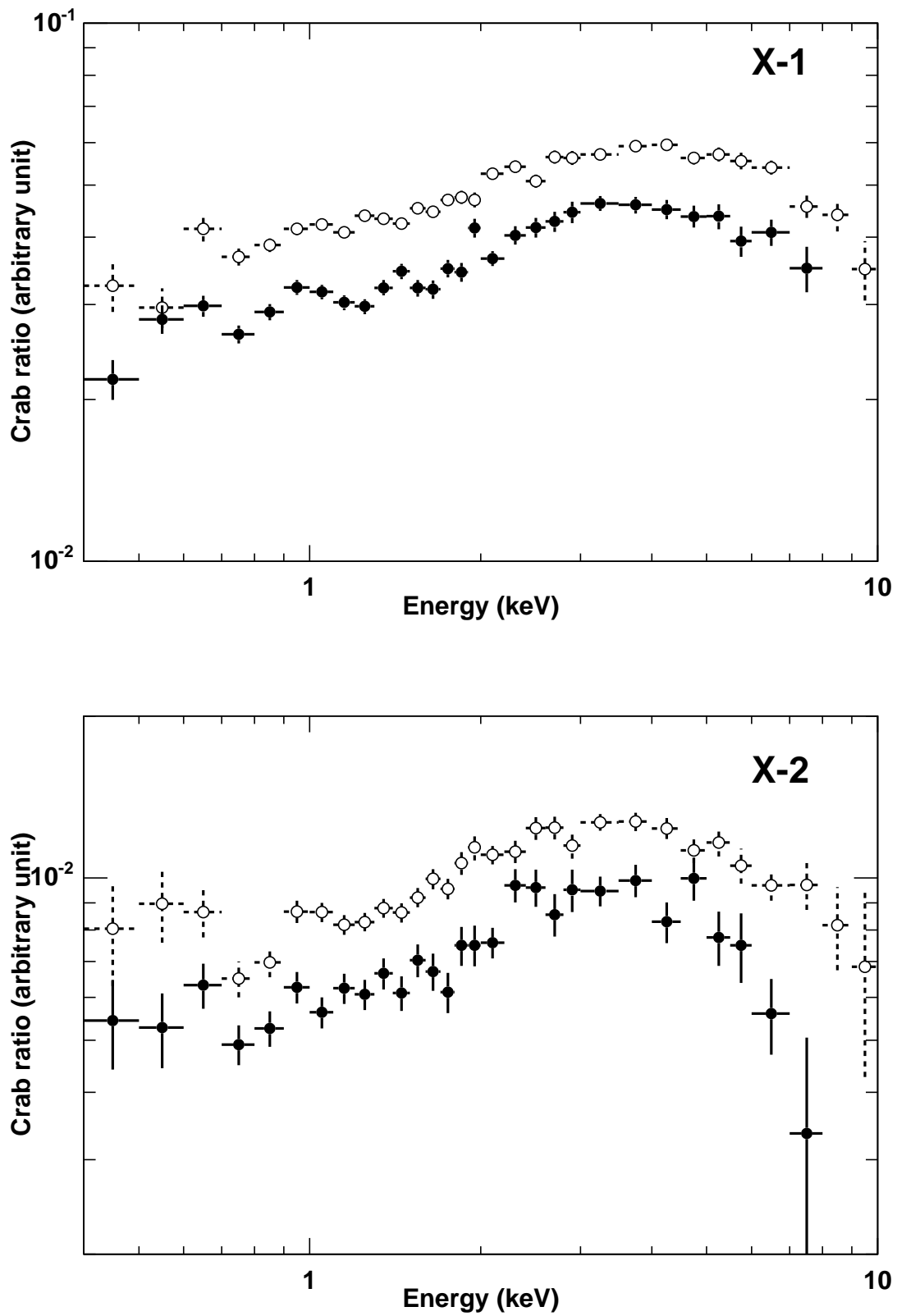


Fig. 4. Crab ratio of the time-averaged spectra for X-1 (top panel) and X-2 (bottom panel), calculated after subtracting the background for two ULXs. Symbols are the same as those of Figure 3. FI data are shifted up for clarity.

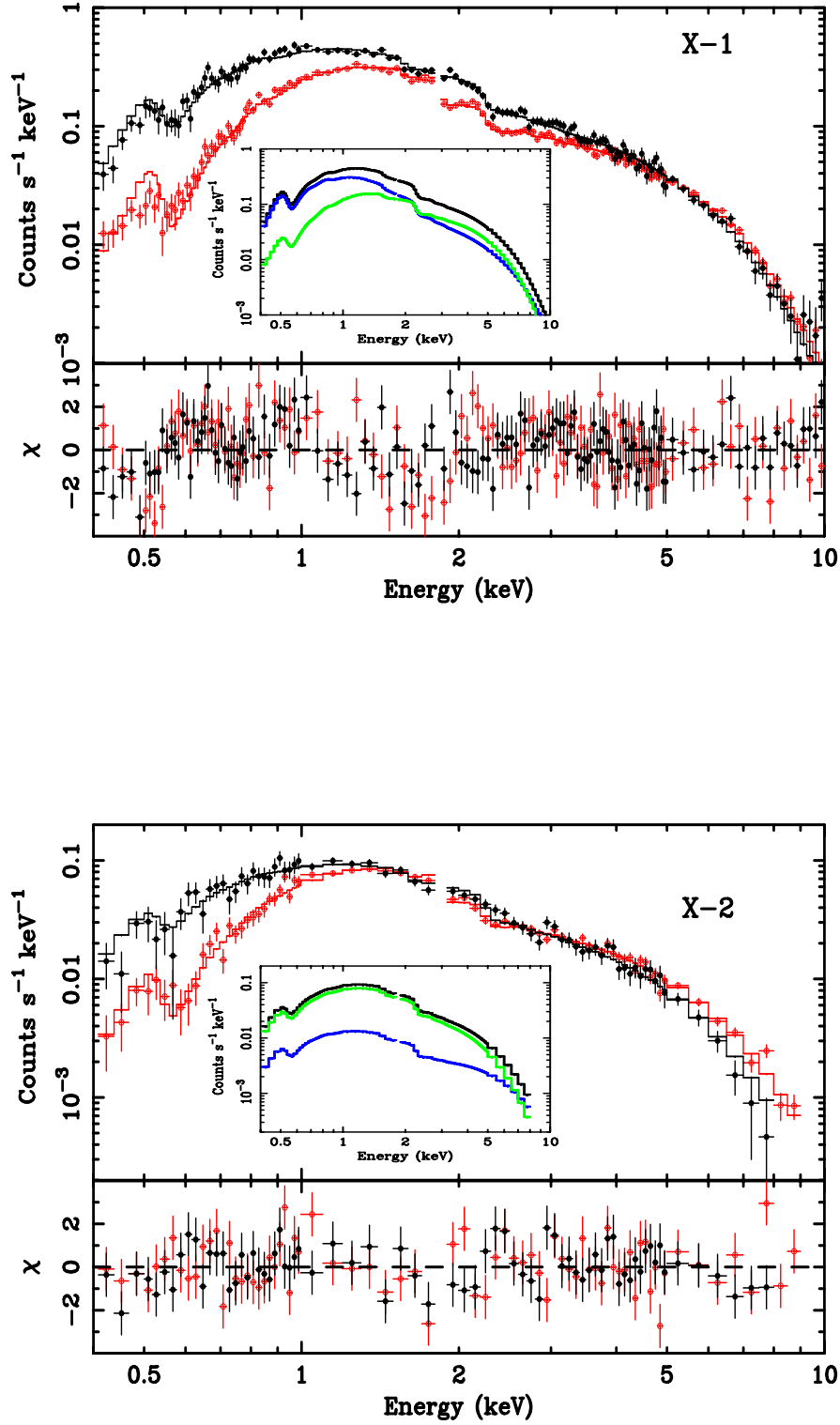


Fig. 5. Time averaged XIS spectra of NGC 1313¹⁹ X-1 (top panel) and X-2 (bottom panel) fitted with the MCD+PL model. The histogram shows the best fit model and crosses represent the observed spectra. The bottom section of each panel shows the fit residuals. The BI (black) and FI (red) spectra are fitted simultaneously except for the relative normalization. The insert shows the best-fit model (black histogram) and contributions of each model (MCD and PL model shown by green and blue histogram, respectively)

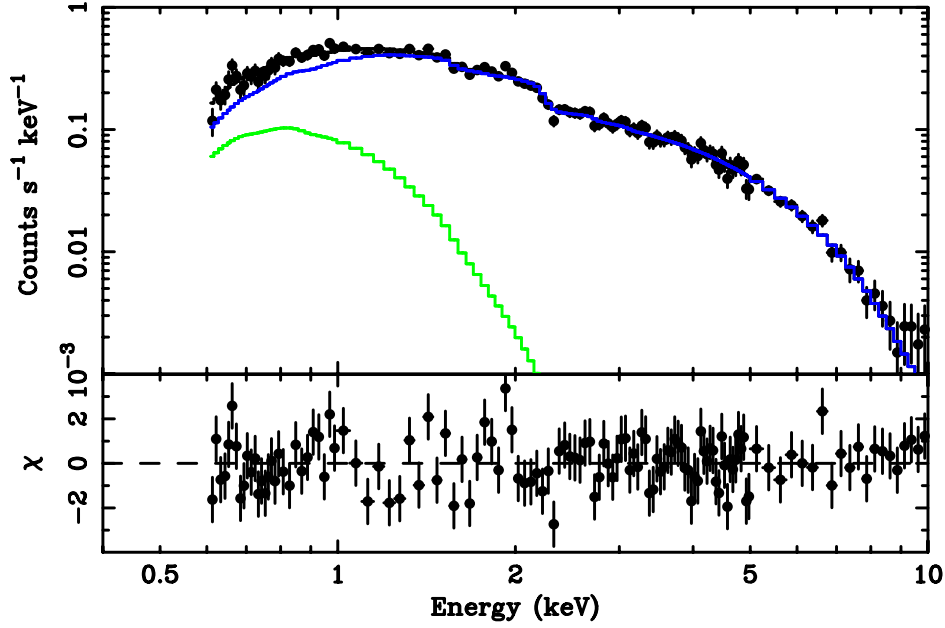
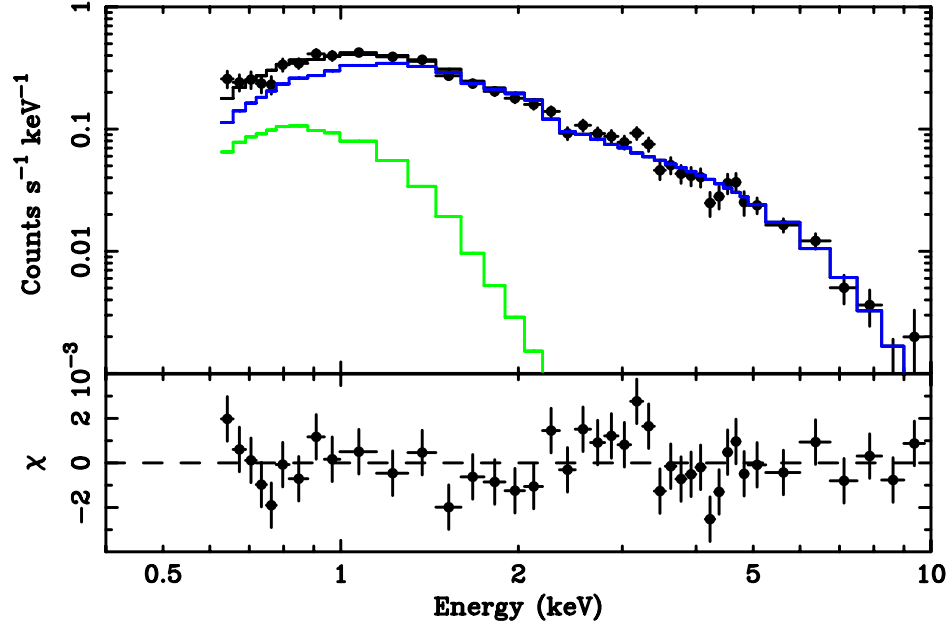


Fig. 6. X-1 spectra for the fainter phase (top panel) and the brighter phase (bottom panel) fitted with the MCD+cutoff-PL model. Symbols are the same as those of figure 5. Contribution of the MCD and cutoff-PL model are given by green and blue histogram, respectively. Only BI sensor data is shown for clarity. Note that data in 1.5–2.3 keV band is not used for the fitting.

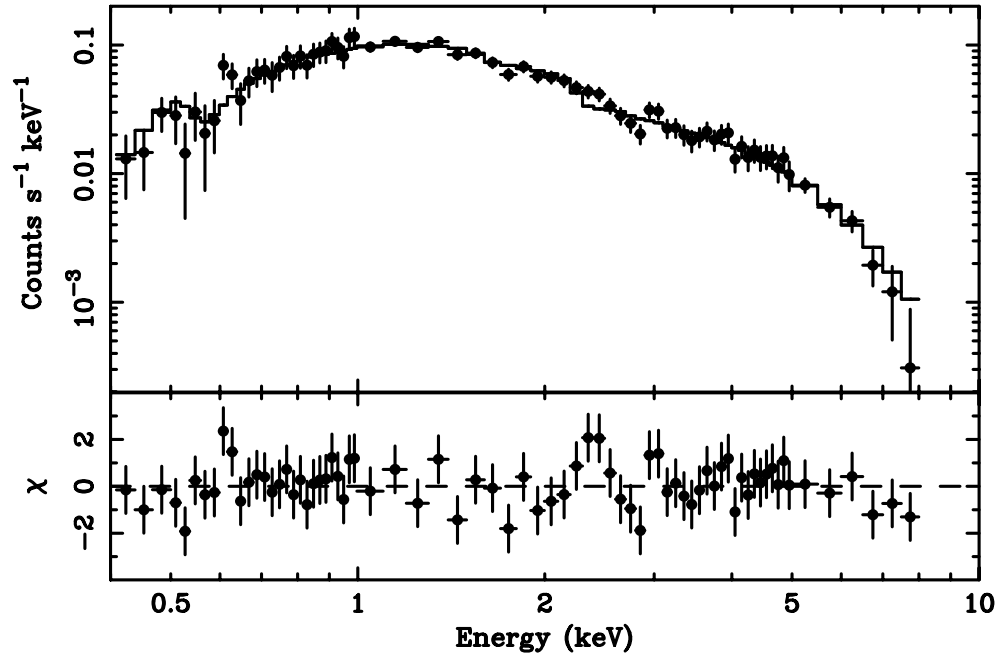
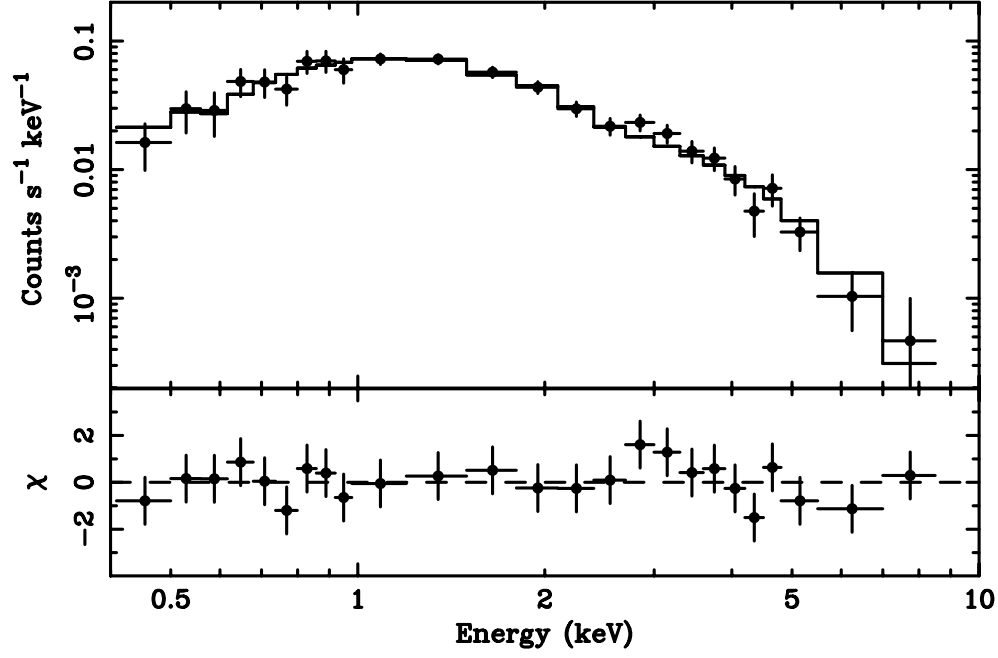


Fig. 7. The same as figure 6, but for X-2 instead of X-1. The fit with the MCD model alone is used for the fainter phase spectrum (top panel) and that with the p -free disk model is used for the brighter one (bottom panel).

References

- Abramowicz, M. A., Czenry, B., Lasota, J. P., & Szuszkiewicz, E. 1988, *ApJ*, 332, 646
- Anders, E., & Ebihara, M. 1982, *Geochimica et Cosmochimica Acta*, 46, 2363-2380
- Baumgartner, W. H. & Mushotzky, R. F. 2006, *ApJ*, 639, 929
- Boldt, E. 1987, *IAU Circ.*, 124, 611
- Colbert, E. J. M., Petre, R., Schlegel, E. M. & Ryder, S. D. 1995, *ApJ*, 446, 177
- Colbert, E. J. M. & Mushotzky, R. F. 1999, *ApJ*, 519, 89
- Cropper, M., Soria, R., Mushotzky, R. F., Wu, K., Markwardt, C. B. & Pakull, M. 2004, *MNRAS*, 349, 39
- Dewangan, G. C., Griffiths, R. E. & Rao, A. R. 2005, *astro-ph/0511112*
- Dewangan, G. C., Griffiths, R. E. & Rao, A. R. 2006, *ApJ*, 641, 125
- Done, K. & Kubota, A. 2005, *astro-ph/0511030*, accepted in *MNRAS*
- Ebisawa, K., Zychi, P, Kubota, A., Mizuno T. & Watarai, K. 2003, *ApJ*, 597, 780
- Fabbiano, G. 1989, *ARA&A*, 27, 87
- Fabbiano, G. & Trinchieri, G. 1987, *ApJ*, 315, 46
- Feng, H. & Kaaret, P. 2005, *ApJ*, 633, 1052
- Feng, H. & Kaaret, P. 2006, *astro-ph/0608066*
- Foschini, L., et al. 2002, *A&A*, 392, 817
- Goad, M. R., Robert, T. P., Reeves, J. N. & Uttley, P. 2006, *MNRAS* 365, 191
- Kobayashi, Y., Kubota, A., Nakazawa, K., Takahashi, T. & Makishima, K. 2003 *PASJ*, 55, 273
- Kokubun, M., et al. 2006, *PASJ*, this volume
- Koyama, K., et al. 2006, *PASJ*, this volume
- Kubota, A., & Done, C. 2004 *MNRAS*, 353, 980
- Kubota, A., Done, C. & Makishima, K. 2002, *MNRAS*, 337, L11
- Kubota, A. & Makishima, K. 2004, *ApJ*, 601, 428
- Kubota, A., Makishima, K. & Ebisawa, K. 2001a *ApJ*, 560, L147
- Kubota, A., Mizuno, T., Makishima, K., Fukazawa, Y., Kotoku, J., Ohnishi, T., and Tashiro, M. 2001b, *ApJ*, 547, L119
- Kubota, A., Tanaka, Y., Makishima, K., Ueda, Y., Dotani, T., Inoue, H. & Yamaoka, K. 1998 *PASJ*, 50, 667
- Makishima, K., et al. 2000, *ApJ*, 535, 632
- McClintock, J. E. & Remillard, R.A. 2003, in *Compact Stellar X-ray Sources*, ed. Lewin, W. H. G. & van der Klis, M. (Cambridge: Cambridge Univ. Press), 157
- Méndez, B., Davis, M., Moustakas, J., Newman, J., Madore, B. F. & Freedman, W. L. 2002 *AJ*, 124, 213
- Miller, J. M., Fabbiano, G., Miller, M. C. & Fabian, A. C. 2003, *ApJ*, 585, L37
- Miller, J. M., Fabian, A. C. & Miller, M. C. 2004, *ApJ*, 607, 931
- Mineshige, S, Hirano, A., Kitamoto, S., Yamada, T., Fukue, J. 1994, *ApJ*, 426, 308
- Mitsuda, K., et al. 1984, *PASJ*, 36, 741
- Mitsuda, K., et al. 2006, *PASJ*, this volume
- Mizuno, T. 2000, Ph.D thesis, Univ. Tokyo

- Mizuno, T., Kubota, A. & Makishima, T. 2001, ApJ, 554, 1282
- Miyamoto, S., Kimura, K., Kitamoto, S., Dotani, T. & Ebisawa, K. 1991, ApJ, 383, 784
- Morrisson, R. & McCammon, D. 1983, ApJ, 270, 119
- Mucciarelli, P., Zampieri, L., Falomo, R., Turolla, R., Treves, A. 2005, ApJ, 633, L101
- Murashima, M., Kubota, A., Makishima, K., Kokubun, M., Hong, Soojing, Negoro, H. 2005, PASJ, 57, 279
- La Parola, V., Peres, G., Fabbiano, G., Kim, D. W. & Bocchino, F. 2001, ApJ556, 47
- Okada, K., Dotani, T., Makishima, K., Mitsuda, K., & Mihara, T. 1998, PASJ, 50, 25
- Roberts, T. P., Warwick, R. S., Ward, M. J., Goad, M. R. & Jenkins, L. P. 2005, MNRAS, 357, 1363
- Roberts, T.P., Kilgard, R.E., Warwick, R.S., Goad, M. R., & Ward, M. J. 2006, astro-ph/0607377, accepted for MNRAS
- Schlegel, E. M., Petre, R., Colbert, E. J. M. & Miller, S. 2000, ApJ, 120, 2373
- Serlemitsos, P., et al. 2006, PASJ, this volume
- Shimura, T. & Takahara, F. 1995, ApJ, 445, 780
- Stobbs, A.-M., Roberts, T. P. & Wilms, J. 2006, MNRAS, 368, 397
- Swartz, D. A., Ghosh, K. K., Tennant, A. F. & Wu, K. 2004, ApJS, 154, 519
- Szuskiewicz, E., Malkan, M. A. & Abramowicz, M. A. 1996, ApJ, 458, 474
- Takahashi, T., et al. 2006, PASJ, this volume
- Toor, A. & Seward, F. D. 1974, ApJ79, 995
- Tully, R. B. 1988, Nearby Galaxies Catalogue (Cambridge: Cambridge Univ. Press)
- Watarai, K., Fukue, J., Takeuchi, M. & Mineshige, S. 2000, PASJ, 52, 133
- Wilms, J., Allen, A. & McCray, R. 2000, ApJ, 542, 914
- Winter, L. M., Mushotzky, R. F. & Reynolds, C. S. 2005, astro-ph/0512480, accepted for ApJ
- Zampieri, L., Mucciarelli, P., Falomo, R., Kaaret, P., di Stefano, R., Turolla, R., Chierigato, M. & Treves, A. 2004, Nuclear Physics B, 132, 387